FEBS Letters 581 (2007) 3783–3788

# H1.X with different properties from other linker histones is required for mitotic progression

Hideaki Takata, Sachihiro Matsunaga, Akihiro Morimoto, Rika Ono-Maniwa, Susumu Uchiyama, Kiichi Fukui*

*Department of Biotechnology, Graduate School of Engineering, Osaka University, Suita 565-0871, Japan*

Received 14 June 2007; accepted 29 June 2007

Available online 10 July 2007

Edited by Ulrike Kutay

**Abstract** **We report here the characterization of H1.X, a human histone H1 subtype. We demonstrate that H1.X accumulates in the nucleolus during interphase and is distributed at the chromosome periphery during mitosis. In addition, the results of fluorescence recovery after photobleaching indicate that the exchange of H1.X on and off chromatin is faster than that of the other H1 subtypes. Furthermore, RNA interference experiments reveal that H1.X is required for chromosome alignment and segregation. Our results suggest that H1.X has important functions in mitotic progression, which are different from those of the other H1 subtypes.**


*Keywords:* Histone H1; Histone H1.X; Chromosome; RNAi; FRAP; Mitosis

## 1. Introduction

Histone H1 stabilizes chromatin structure by binding close to the entry–exit sites of linker DNA [1] and is thought to be important for chromatin condensation and the chromatin higher structure. In fact, depletion of histone H1 leads to structural and functional defects of chromosomes [2,3] and affects proper embryonic development [4]. In mammals, 10 H1 subtypes have been reported to date, i.e., H1.1–H1.5 [5,6], H1° [7], H1.t [8], H1Foo [9], HILS1 [10] and H1.X [11].

Our previous studies of human metaphase chromosomes indicated that H1.X is a structural component of chromosomes [12,13]. H1.X expression is commonly detected throughout human tissues [11]. Its amino acid sequence does not show high similarities with the other somatic histone H1 subtypes (~30%), although it does possess some of the characteristic features of linker histones [14]. In addition, H1.X is partially associated with nucleosomes and enriched in micrococcal nuclease-resistant chromatin [15].

In the present study, we analyzed the function of H1.X in mitosis, since the biological functions of H1.X have not yet been elucidated. We demonstrate by fluorescence recovery after photobleaching (FRAP) and RNA interference (RNAi) analyses that H1.X has distinct properties from the other H1 subtypes that are essential for mitotic progression.

## 2. Materials and methods

### 2.1. Cells and transfection

HeLa cells were grown in Dulbecco's modified Eagle's medium (GIBCO BRL) supplemented with 10% fetal bovine serum (Equitech-Bio Inc.). For construction of a cell line stably expressing GFP-H1.X, a cDNA of H1.X was inserted into a pEGFP-C1 vector (Clontech), and the resulting plasmid encoding H1.X-GFP was transfected into HeLa cells using the FuGene6 reagent (Roche). A GFP-tagged expression vector for H1.2 visualization was constructed by integration of a human H1.2 cDNA into pEGFP-C1.

### 2.2. Antibodies

The primary antibodies used were: anti-H1.X rabbit polyclonal (Abcam), 1:200 dilution; anti-nucleolin mouse monoclonal (Upstate Biotechnology), 1:50 dilution; anti-α-tubulin mouse monoclonal (Calbiochem), 1:100 dilution; anti-γ-tubulin rabbit polyclonal (Sigma), 1:2000 dilution; anti-Bub1 mouse monoclonal (MBL), 1:20 dilution; anti-BubR1 mouse monoclonal (BD Transduction Laboratories), 1:1000 dilution; anti-MAD2 rabbit polyclonal (Covance), 1:100 dilution; and CREST (Cortex Biochem), 1:1000 dilution.

### 2.3. RNAi

A small interfering RNA (siRNA) duplex for H1.X (5′-CCAAGAAGGUUCCGUGGUUTT-3′) was chemically synthesized and HeLa cells were transfected with 120 nM of the siRNA duplex using Lipofectamine 2000 (Invitrogen), according to the manufacturer's instructions. A control siRNA duplex (5′-UUCUCCGAACGUGUCACGUTT-3′; Qiagen) was used for control transfections. Cells were collected at 48 h after transfection and used for further analysis.

### 2.4. Immunofluorescence microscopy

HeLa cells grown on coverslips were fixed with 4% paraformaldehyde in PBS (pH 7.4) for 15 min at 37 °C, and then permeabilized with 0.2% Triton X-100 in PBS for 10 min at room temperature. After incubation with 1% BSA-PBS for 15 min, the cells were incubated with a primary antibody for 1 h at room temperature, followed by incubation with an appropriate secondary antibody for 1 h. The secondary antibodies (labeled with Alexa 488 or TRITC) were used at a dilution of 1:200. After washing, the cells were stained with 1 μg/ml 4′,6-diamidino-2-phenylindole (DAPI) and observed under an Axioplan II imaging fluorescence microscope (Carl Zeiss). Deconvoluted images were captured with a cooled CCD camera (CH 350/L; Roper Scientific) using an IX-70 microscope (Olympus) and analyzed using the Delta vision software (Applied Precision).

*Corresponding author. Fax: +81 6 6879 7442.
*E-mail address:* kfukui@bio.eng.osaka-u.ac.jp (K. Fukui).

*Abbreviations:* RNAi, RNA interference; siRNA, small interfering RNA; GFP, green fluorescent protein; FRAP, fluorescence recovery after photobleaching; DAPI, 4′, 6-diamidino-2-phenylindole; NEBD, nuclear envelope breakdown

0014-5793/$32.00 
doi:10.1016/j.febslet.2007.06.076

Metaphase chromosome spreads were prepared as described previously [12].

*2.5. FRAP analysis*

FRAP analysis was performed using an IX-71 inverted microscope (Olympus) equipped with an FV300 scanning unit. First, a single image was captured by the 488 nm-line of a 10 mW-argon laser (set to 1%) and then a selected area ($2.3 \times 2.3\ \mu m^2$) was bleached by the 488 nm-line of the argon laser (set to 40%). After 3 s of photobleaching, images were captured using the same scanning settings as above at intervals of 1.1 s (GFP-H1.X) or 20 s (GFP-H1.2). The relative intensities were calculated as follows:

$$\text{Relative intensity} = (I_t/W_t)/(I_0/W_0)$$

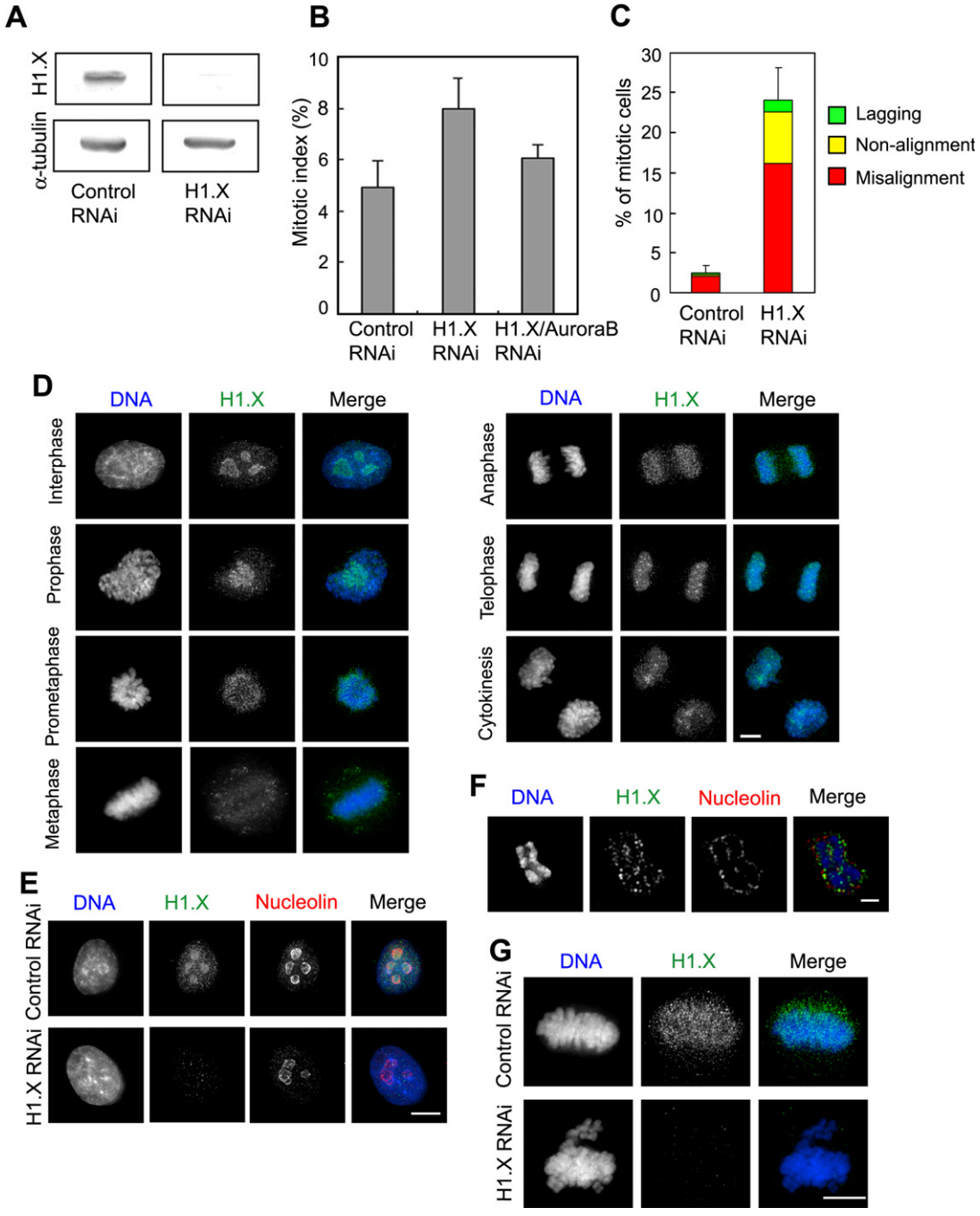


Fig. 1. Mitotic defects in H1.X-depleted cells and localization of H1.X during the cell cycle. (A) Efficient repression of H1.X after RNAi treatment was confirmed by immunoblotting. The expression of α-tubulin was used as a control. (B) The mitotic indexes in control and H1.X RNAi cells were calculated after immunostaining with an anti-α-tubulin antibody. The mitotic index in H1.X and Aurora B double-knockdown cells was also calculated. $n = 5$; >1000 cells were counted. (C) Chromosome aberrations were categorized into three groups: misalignment, non-alignment and lagging chromosomes. (D) HeLa cells were fixed with 4% paraformaldehyde and stained with an anti-H1.X antibody (green) at different mitotic phases. DNA was stained with DAPI (blue). Bar, 5 μm. (E) The nucleolar localization of H1.X (green) was confirmed by counterstaining for nucleolin (red). Bar, 5 μm. (F) Localization of H1.X to the chromosome periphery. Metaphase chromosome spreads were stained with anti-H1.X (green) and anti-nucleolin (red) antibodies. Bar, 1 μm. (G) Typical metaphase chromosome images in control and H1.X RNAi mitotic cells stained with DAPI (blue) and an anti-H1.X antibody (green). Bar, 5 μm.

where $I_0$ is the average intensity in the region of interest before photobleaching, $I_t$ is the average intensity in the region of interest at time point $t$, $W_0$ is the average intensity in both photobleached and non-photobleached regions before photobleaching and $W_t$ is the average intensity in both photobleached and non-photobleached regions at time point $t$. The $t_{1/2}$ value was defined as the time required to reach half-maximum recovery and calculated from the corrected recovery curves.

## 3. Results

### 3.1. H1.X is required for accurate mitotic progression

To examine the biological function of H1.X, we performed RNAi of H1.X. Immunoblot and immunofluorescence analyses revealed that the abundance of H1.X was greatly decreased (Fig. 1A, E and G). The specificity of the anti-H1.X antibody used in this study was confirmed by immunoblotting (Fig. S1A). Furthermore, H1.X depletion had no influence on the expression of H1.2 (Fig. S1F). As shown in Fig. 1B, the mitotic index was elevated to $8.0 \pm 1.2\%$ in H1.X RNAi cells, compared to $4.9 \pm 1.0\%$ in control RNAi cells ($p < 0.05$). In H1.X-depleted cells, chromosome condensation occurred normally, and there was no influence on the localizations of known chromosomal proteins, namely hCAPE, topoisomerase IIα, CENPA, CENPE and CENPF (Fig. S2). However, chromosome alignment at the metaphase plate was impaired by H1.X depletion (Fig. 1C and G). We categorized the defects in chromosome alignment into the following two groups: misalignment chromosomes (1–10 chromosomes were not aligned at the metaphase plate, whereas the majority of the chromosomes were aligned) and non-alignment chromosomes (>10 chromosomes were not aligned at the metaphase plate or chromosomes were scattered throughout the cytoplasm). The misalignment and non-alignment chromosomes were detected in 16.1% and 6.5% of H1.X-depleted mitotic cells, respectively, compared to the corresponding values of 2.1% and 0.2% of control cells. In addition, lagging chromosomes were observed at anaphase in 1.4% of H1.X-depleted mitotic cells, compared to 0.2% of control cells. These defects in chromosome dynamics and mitotic progression were also observed in living cells (Fig. S3). The above phenotypes of H1.X-depleted cells were found to be reproducible when similar RNAi experiments were carried out using another siRNA sequence for H1.X (Fig. S1B-E).

### 3.2. Histone H1.X is localized to nucleoli and mitotic chromosomes

To examine the intracellular localization of H1.X, we performed immunostaining with an anti-H1.X antibody (Fig. 1D). H1.X was predominantly localized in the nucleoli of interphase cells. The precise nucleolar localization of H1.X was confirmed by counterstaining of the nucleolar proteins nucleolin and fibrillarin. The nucleolar localization pattern of H1.X differed from those of nucleolin and fibrillarin (Figs. 1E and S1G). The signal intensity of H1.X in the nucleoli was significantly decreased following depletion of H1.X.

During mitosis, H1.X was distributed on chromosomes, especially at the chromosome periphery (Fig. 1F). In H1.X RNAi cells, the H1.X signals around the chromosomes disappeared and chromosome misalignment was observed (Fig. 1G).

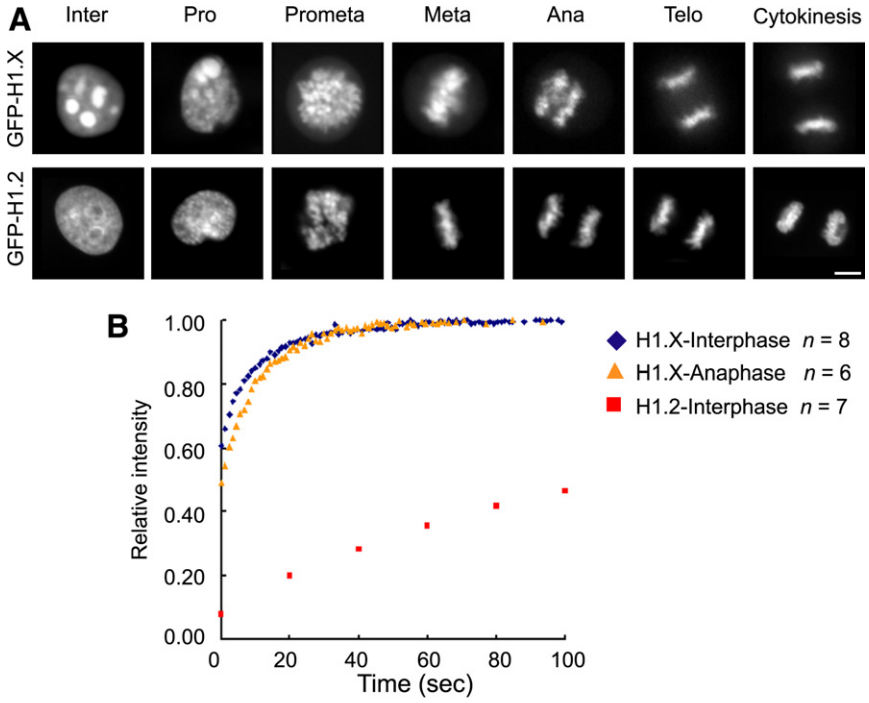


Fig. 2. H1.X dynamics during the cell cycle. (A) Comparison of the localization patterns of GFP-H1.X and GFP-H1.2 in living HeLa cells throughout the cell cycle. Bar, 5 μm. (B) FRAP recovery curves for GFP-H1.X at interphase (blue) and anaphase (orange). The FRAP recovery curve for GFP-H1.2 at interphase (red) is also indicated. The plot shows the relative recovery of fluorescence in the photobleached region *versus* time.

### 3.3. H1.X is dynamically associated with chromatin

To observe the dynamics of H1.X in living cells, we developed a stable HeLa cell line that constitutively expressed H1.X fused to enhance green fluorescent protein (EGFP) at its N-terminus. GFP-H1.X was mainly localized in nucleoli at interphase and chromosomes during mitosis (Fig. 2A). The localization pattern of H1.X differed from that of the typical linker histone H1.2. At interphase, histone H1.2 was mainly localized in the nucleoplasm (Fig. 2A). During mitosis, GFP-H1.2 signals were detected in the chromosomes, and not in the cytoplasm.

To quantitatively measure the binding kinetics of H1.X to unperturbed chromatin in living cells, we performed a FRAP analysis. As shown in Fig. 2B, the fluorescence recovery rate of H1.X ($t_{1/2} = 4.7 \pm 1.9$ s) was significantly faster than that of H1.2 ($t_{1/2} = 126.9 \pm 24.1$ s). Consistent with these findings, endogenous H1.X was dissociated from chromatin by a lower concentration of NaCl than H1.2 (data not shown). Thus, the interaction between H1.X and chromatin is considerably weaker than that between chromatin and H1.2. We found that the exchange rate of H1.X remained unchanged between interphase and anaphase. This observation was in strong contrast to the property of H1.2, which shows dynamic changes in its chromatin binding persistency during the cell cycle [16].

### 3.4. Depletion of H1.X induces aberrant spindle formation

The prolonged mitosis observed in H1.X-depleted cells (Fig. S3) suggests that the spindle checkpoint is activated by the depletion of H1.X. Actually, spindle checkpoint proteins, including Bub1, BubR1 and Mad2, were accumulated at the kinetochores of misaligned chromosomes (Fig. 3A), while the expression levels of cell cycle-related proteins required for the transition from metaphase to anaphase, namely CDC20, CDC27 and Plk1, were the same as those in control cells (Fig. S4B and C). Furthermore, double knockdown of H1.X with Aurora B, one of the spindle checkpoint proteins, de-

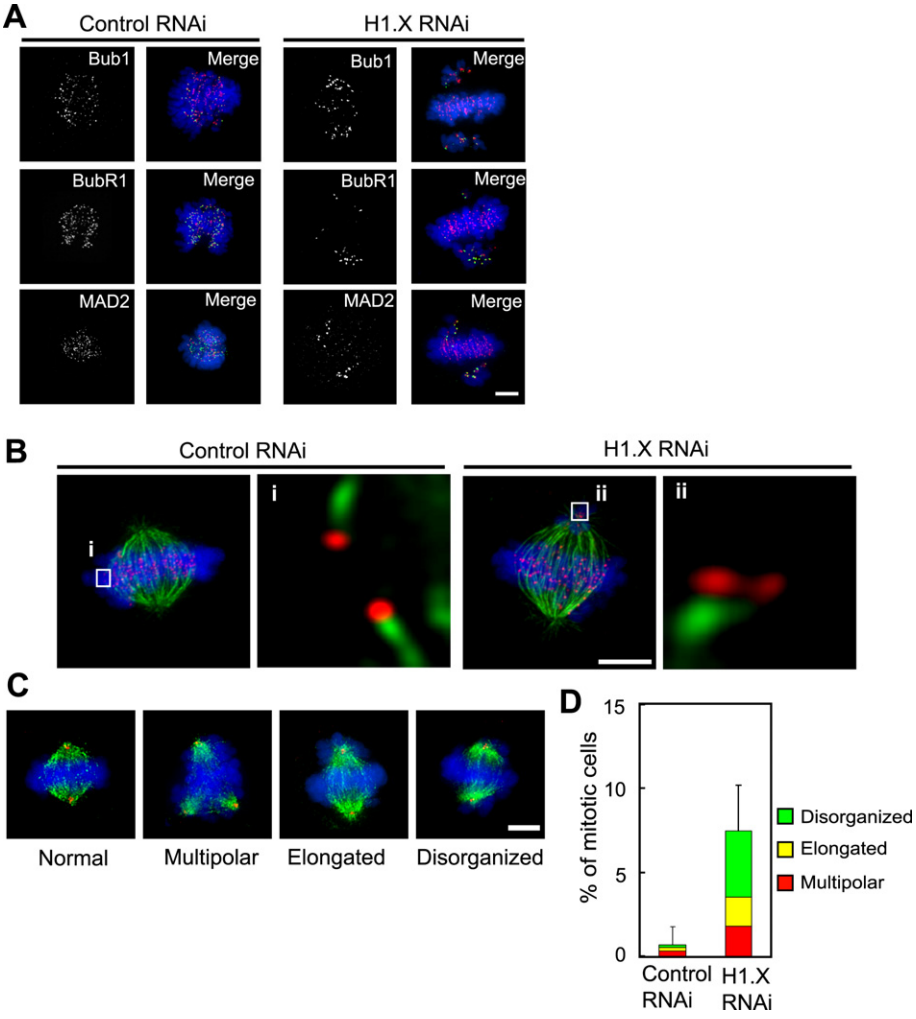


Fig. 3. Microtubule attachment and mitotic spindle morphology. (A) Localizations of spindle checkpoint proteins (green), Bub1, BubR1 and MAD2, in control cells at prometaphase and in H1.X RNAi cells. Kinetochores were detected by CREST (red) and DNA was stained with DAPI (blue). Bar, 5 μm. (B) Kinetochore fiber formation was examined by staining with an anti-α-tubulin antibody (green), CREST (red) and DAPI (blue). The enlarged figures show optically sectioned images of microtubule–kinetochore attachments to an aligned chromosome in a control cell (i) and a misaligned chromosome in an H1.X-depleted cell (ii). Bar, 5 μm. (C) Three types of aberrant spindle morphologies are observed in H1.X-depleted cells. Microtubules were stained with an anti-α-tubulin antibody (green) and spindle poles were stained with an anti-γ-tubulin antibody (red). (D) Frequencies of the three phenotypes of spindle aberrations. $n = 5$; >1000 cells were counted in each experiment.

creased the mitotic index from 8.0% to 6.1% in H1.X-depleted cells (Fig. 1B). These results indicate that the mitotic arrest caused by H1.X depletion was due to spindle checkpoint activation rather than failure of metaphase exit.

To further examine whether H1.X is required for accurate attachment of microtubules to kinetochores, we analyzed kinetochore fiber formation in RNAi cells. In control cells, end-on attachments of microtubules to the kinetochores from the opposite spindle poles were clearly observed (Fig. 3B). In contrast, syntelic attachments were detected in misaligned chromosomes after H1.X depletion. In addition, three types of defect in spindle morphology were observed (Fig. 3C and D). In multipolar cells, more than three spindle poles were detected. This phenotype was observed in 1.8% of H1.X-depleted mitotic cells, compared to 0.4% of control cells. The most frequently observed defect in spindle morphology was spindle disorganization. In this case, the mitotic spindle appeared less focused and the symmetric formation of the spindle was impaired. Spindle disorganization was observed in 3.9% of H1.X-depleted mitotic cells, compared to 0.2% of control cells. The inter-centrosome distance was increased in 1.7% of mitotic H1.X-depleted cells. These results strongly suggest that H1.X is required for accurate mitotic spindle formation.

## 4. Discussion

We have demonstrated that H1.X is localized in nucleoli by immunostaining with an anti-H1.X antibody and observation of GFP-tagged H1.X (Figs. 1 and 2), whereas a somatic H1 subtype, H1.2, is not localized in nucleoli. The alternative localization of H1.X implies a relationship with nucleolar functions, such as rDNA transcription and rRNA maturation. However, depletion of H1.X did not affect the localizations of nucleolin and fibrillarin (Figs. 1E and S1G), suggesting that H1.X is not required for the nucleolar structure.

We found that H1.X has low chromatin binding activity and exhibits rapid exchange from chromatin compared with H1.2. Recent FRAP analyses have indicated that H1 is dynamically associated with chromatin in vivo and that both the globular and C-terminal domains of H1 are required for its stable association with the nucleosome [17–19]. The C-terminal domain of each H1 subtype is thought to play a role in determining its binding properties, because the features of this domain, such as the number of lysine residues, differ greatly among individual H1 subtypes [20]. For example, 40% of the amino acids in this domain in H1.2 are occupied by two basic amino acids (Lys or Arg), but this proportion is reduced to 33% in H1.X. Furthermore, Thr152 and Ser183, which are important for accurate H1–chromatin interactions [18], are not conserved in H1.X. These features of H1.X are probably responsible for the weaker binding activity between H1.X and chromatin.

H1.X is preferentially distributed to the chromosome periphery, which frequently contains nucleolar components [21], suggesting that H1.X has particular functions at the chromosome periphery. Our previous study on nucleolin, another chromosome peripheral protein, indicated that the integrity of the chromosome periphery is important for chromosome dynamics and cell cycle progression [22]. We did not detect any morphological defects of mitotic chromosomes in H1.X-depleted cells. However, mitotic progression was severely inhibited and defects in chromosome alignment, chromosome segregation and spindle morphology were observed. Moreover, depletion of H1.X disturbed microtubule attachment to the kinetochores. Taken together, H1.X has different localization patterns and chromatin binding activity compared to the other linker histones throughout the cell cycle and its function is essential for mitotic progression.

*Acknowledgements:* This work was supported by a Special Coordination Fund to K.F. and Grants-in-Aid for Scientific Research from the Ministry of Education, Science, Culture, Sports, Science and Technology of Japan to S.M. and S.U. and by an Industrial Technology Research Grant Program in 2003 from the New Energy and Industrial Technology Development Organization (NEDO) of Japan to S.M.

## Appendix A. Supplementary data

Supplementary data associated with this article can be found, in the online version, at doi:10.1016/j.febslet.2007.06.076.

## References

[1] van Holde, K.E. (1989) Chromatin, Springer-Verlag, New York, NY.
[2] Shen, X., Yu, L., Weir, J.W. and Gorovsky, M.A. (1995) Linker histones are not essential and affect chromatin condensation in vivo. Cell 82, 47–56.
[3] Maresca, T.J., Freedman, B.S. and Heald, R. (2005) Histone H1 is essential for mitotic chromosome architecture and segregation in *Xenopus laevis* egg extracts. J. Cell Biol. 169, 859–869.
[4] Fan, Y., Nikitina, T., Morin-Kensicki, E.M., Zhao, J., Magnuson, T.R., Woodcock, C.L. and Skoultchi, A.I. (2003) H1 linker histones are essential for mouse development and affect nucleosome spacing in vivo. Mol. Cell Biol. 23, 4559–4572.
[5] Rasheed, B.K., Whisenant, E.C., Ghai, R.D., Papaioannou, V.E. and Bhatnagar, Y.M. (1989) Biochemical and immunocytochemical analysis of a histone H1 variant from the mouse testis. J. Cell Sci. 94, 61–71.
[6] Parseghian, M.H., Henschen, A.H., Krieglstein, K.G. and Hamkalo, B.A. (1994) A proposal for a coherent mammalian histone H1 nomenclature correlated with amino acid sequences. Protein Sci. 3, 575–587.
[7] Khochbin, S. and Wolffe, A.P. (1994) Developmentally regulated expression of linker-histone variants in vertebrates. Eur. J. Biochem. 225, 501–510.
[8] Seyedin, S.M., Cole, R.D. and Kistler, W.S. (1981) H1 histones from mammalian testes. The widespread occurrence of H1t. Exp. Cell Res. 136, 399–405.
[9] Tanaka, M., Hennebold, J.D., Macfarlane, J. and Adashi, E.Y. (2001) A mammalian oocyte-specific linker histone gene H1oo: homology with the genes for the oocyte-specific cleavage stage histone (cs-H1) of sea urchin and the B4/H1M histone of the frog. Development 128, 655–664.
[10] Yan, W., Ma, L., Burns, K.H. and Matzuk, M.M. (2003) HILS1 is a spermatid-specific linker histone H1-like protein implicated in chromatin remodeling during mammalian spermiogenesis. Proc. Natl. Acad. Sci. USA 100, 10546–10551.
[11] Yamamoto, T. and Horikoshi, M. (1996) Cloning of the cDNA encoding a novel subtype of histone H1. Gene 173, 281–285.
[12] Uchiyama, S., Kobayashi, S., Takata, H., Ishihara, T., Hori, N., Higashi, T., Hayashihara, K., Sone, T., Higo, D., Nirasawa, T., Takao, T., Matsunaga, S. and Fukui, K. (2005) Proteome analysis of human metaphase chromosomes. J. Biol. Chem. 280, 16994–17004.
[13] Takata, H., Uchiyama, S., Nakamura, N., Nakashima, S., Kobayashi, S., Sone, T., Kimura, S., Lahmers, S., Granzier, H., Labeit, S., Matsunaga, S. and Fukui, K. (2007) A comparative proteome analysis of human metaphase chromosomes isolated from two different cell lines reveals a set of conserved chromosome-associated proteins. Genes Cells 12, 269–284.

[14] Cole, R.D. (1987) Microheterogeneity in H1 histones and its consequences. Int. J. Pept. Protein Res. 30, 433–449.
[15] Happel, N., Schulze, E. and Doenecke, D. (2005) Characterisation of human histone H1x. Biol. Chem. 386, 541–551.
[16] Chen, D., Dundr, M., Wang, C., Leung, A., Lamond, A., Misteli, T. and Huang, S. (2005) Condensed mitotic chromatin is accessible to transcription factors and chromatin structural proteins. J. Cell Biol. 168, 41–54.
[17] Misteli, T., Gunjan, A., Hock, R., Bustin, M. and Brown, D.T. (2000) Dynamic binding of histone H1 to chromatin in living cells. Nature 408, 877–881.
[18] Hendzel, M.J., Lever, M.A., Crawford, E. and Th'ng, J.P. (2004) The C-terminal domain is the primary determinant of histone H1 binding to chromatin in vivo. J. Biol. Chem. 279, 20028–20034.
[19] Brown, D.T., Izard, T. and Misteli, T. (2006) Mapping the interaction surface of linker histone H1(0) with the nucleosome of native chromatin in vivo. Nat. Struct. Mol. Biol. 13, 250–255.
[20] Ponte, I., Vidal-Taboada, J.M. and Suau, P. (1998) Evolution of the vertebrate H1 histone class: evidence for the functional differentiation of the subtypes. Mol. Biol. Evol. 15, 702–708.
[21] van Hooser, A.A., Yuh, P. and Heald, R. (2005) The perichromosomal layer. Chromosoma 114, 377–388.
[22] Ma, N., Matsunaga, S., Takata, H., Ono-Maniwa, R., Uchiyama, S. and Fukui, K. (2007) Nucleolin functions in nucleolus formation and chromosome congression. J. Cell Sci. 120, 2091–2105.